Unanticipated Inhibition of the Metallo-β-lactamase from *Bacteroides fragilis* by 4-Morpholineethanesulfonic Acid (MES): A Crystallographic Study at 1.85-Å Resolution‡

Paula M. D. Fitzgerald,* Joseph K. Wu, and Jeffrey H. Toney

Department of Biochemistry, Merck Research Laboratories, Rahway, New Jersey 07065

Received December 10, 1997; Revised Manuscript Received February 24, 1998

ABSTRACT: As part of a structure-aided effort to design clinically useful inhibitors of metallo-β-lactamases, the X-ray crystal structure of a complex between the metallo-β-lactamase from *Bacteroides fragilis* and 4-morpholinoethanesulfonic acid (MES) has been determined and a model for the structure has been refined to a crystallographic *R*-factor of 0.151 for data between 10.0- and 1.85-Å resolution. Although the binding of MES was an adventitious result of the use of MES as a buffer in the crystallization mixture, MES was subsequently shown to be a competitive inhibitor of the enzyme, with a K_i of 23 ± 5 mM. MES binds in the same fashion to both of the molecules in the crystallographic asymmetric unit; both direct and solvent-mediated hydrogen bonds to the protein and to the binuclear zinc cluster are observed, involving the oxygens of the sulfonic acid group and the nitrogen of the morpholino ring. In addition, there are hydrophobic interactions between the morpholino ring and residues in the flexible β-strand of the enzyme between residues 26 and 36. Comparison of this structure with the previously reported unliganded structures of the same enzyme [Concha, N. O., Rasmussen, B. A., Bush, K., and Herzberg, O. (1996) *Structure 4*, 823−836; Carfi, A., Duée, E., Paul-Soto, R., Galleni, M., Frère, J.-M., and Dideberg, O. (1998) *Acta Crystallogr. D54*, 47−57] reveals that although the overall conservation of structure in the three different crystal lattices is very high, binding of MES is correlated with a significant change in the conformation of this β-strand. The flexibility of this β-strand will be an important consideration in the design of inhibitors of the metallo-β-lactamases.

Antibiotics of the carbapenem class are highly effective against a wide spectrum of bacterial infections (*1*), but increasingly their effectiveness is being challenged by the emergence of strains of bacteria resistant to this class of compounds (*2*). One mechanism by which bacteria become resistant is the expression of an enzyme capable of hydrolyzing the carbapenems, thus rendering them ineffective. Although several class A β-lactamases have been shown to express hydrolytic activity against carbapenems and related antibiotics, the majority of the β-lactamases characterized to date as conferring resistance to carbapenems are members of the class B family (*3*). Unlike the other classes of β-lactamase, which have serine as the catalytically essential residue, the class B enzymes have zinc at the catalytic center, and are thus known as metallo-β-lactamases.

The metallo-β-lactamases provide a target for therapeutic intervention in the treatment of infections involving carbapenem-resistant strains of bacteria. To understand the activity of the enzyme, and to aid in a program of structure-aided drug design, the structures of these enzymes have been determined from two different bacteria. The structure of the metallo-β-lactamase from *Bacillus cereus* (*4*) revealed that the enzyme has a molecular fold that had not previously been observed. The enzyme has two domains of roughly equivalent topology, with each domain consisting of a multistranded β-sheet with α-helices on one face; the β-sheets from the two domains pack against one another, with the active site at the top of the resulting β-sandwich. The active site in the original report of the *B. cereus* structure contained a single zinc atom (*4*), but subsequent structural studies of the same enzyme (*5*), and of the enzyme from *Bacteroides fragilis* (*6*, *7*), have revealed that there are two zinc atoms in the active site.

A notable feature of both the *B. cereus* and *B. fragilis* metallo-β-lactamase structures is the flexibility of a region of 11 residues in the N-terminal domain. In the *B. cereus* structure, there is no interpretable density for eight of these residues, but in the tetragonal form of the unliganded *B. fragilis* structure (*6*), all but two of the residues are ordered, and the conformation of this region is a β-strand. The more recently reported orthorhombic form of the unliganded *B. fragilis* structure (*7*) has all residues in this β-strand ordered, in a conformation stabilized by crystal packing interactions. Given the close proximity of this strand to the active site zinc cluster, it may well play a role in interacting with substrates (or inhibitors), and a knowledge of its conformation in an inhibited complex should greatly aid the process of structure-aided drug design.

‡ Coordinates have been deposited with the Brookhaven Protein Data Bank (entry code 1A7T).

* To whom correspondence should be addressed: P.O. Box 2000 (RY50-105), Rahway, NJ 07065. Voice: (732) 594-5510. Fax: (732) 594-5042. E-mail: paula_fitzgerald@merck.com.

S0006-2960(97)03033-X CCC: $15.00
Published on Web 04/28/1998

We report here the structure of such an inhibited complex, between the buffer 4-morpholineethanesulfonic acid (MES)[1] and the metallo-β-lactamase from *B. fragilis*. Crystallization of this complex was an unexpected consequence of the presence of MES as the buffer in the crystallization mixture, but we present data to show that MES is indeed an inhibitor (albeit a weak one) of the enzyme. In the complex, all residues in the flexible β-strand between residues 26 and 36, which we shall hereinafter refer to as the flap, are ordered, and the side chains of three residues in the flap do indeed interact directly with the inhibitor. We have compared the conformations of the flap observed in the MES complex to the conformations seen in the unliganded structures of the same enzyme (*6*−*7*), and we find them to be significantly different. Flexibility of the flap may well be a crucial component in the interactions of metallo-β-lactamases with inhibitors.

MATERIALS AND METHODS

Computer Programs. X-ray diffraction data were integrated, merged, and scaled using the program XENGEN (*8*). Rotation function calculations were performed using the MERLOT program package (*9*). Heavy-atom refinement, solvent flattening, and electron density map calculations were performed using the program PHASES (*10*). The structure was refined using the program X-PLOR (*11*), as well as a version of the PROTIN/PROLSQ suite of programs (*12*) that had been heavily modified for local use. Electron density maps were fit using the program CHAIN (*13*). Three-dimensional α-carbon positions were calculated from stereo diagrams using the program STEREO by M. G. Rossmann. A model for the inhibitor was built using the program AFS (a Merck proprietary program that is an extension of the work described in refs *14* and *15*). Target values for the least-squares restraint of the inhibitor structure during crystallographic refinement were generated from this model and added to the PROTIN ideals file using a locally modified version of the program CONEXN (*16*). The stereochemical quality of the model was assessed using the program PROCHECK (*17*). Structure comparisons were performed with the locally written program RGBSUP; this program first calculates the best rigid-body alignment of two coordinate sets and then systematically eliminates from the fit atom pairs that differ by more than a user-specified limit. Illustrations for this manuscript were created with the program CHAIN, locally developed software, and Adobe Illustrator (Adobe Systems, Mountain View, CA).

Nomenclature Used for the Structure. As translated in vivo, the sequence of the metallo-β-lactamase from *B. fragilis* contains 249 amino acids. The first 17 of these amino acids are a putative periplasmic signaling sequence, which is cleaved during the maturation of the enzyme. We have selected a numbering scheme that begins at the amino terminus of the 232-residue mature protein, with the sequence AQKSVK, as this is the amino terminus of the construct from which the protein used in the study was expressed. This numbering scheme is consistent with the one used in the report of the crystal structure of the metallo-β-lactamase from *B. cereus* (*4*) and with the one used in the report of the orthorhombic crystal form of the unliganded metallo-β-lactamase from *B. fragilis* (*7*), both of which take the first residue of the mature protein as residue 1, but differs from the scheme used in the tetragonal structure of the unliganded *B. fragilis* enzyme (*6*), which takes the first residue of the signaling sequence as residue 1. In the crystal structures described in the present report, the two molecules in the crystallographic asymmetric are designated molecule A and molecule B. There are two zinc atoms within the active site of each molecule; we refer to the zinc atom that has ligands His 82, His 84, and His 145 as Zn 1 and to the zinc atom that has ligands Asp 86, Cys 164, and His 206 as Zn 2.

Crystallization. The cloning, expression, and purification of the metallo-β-lactamase from a clinical isolate of *B. fragilis* was described previously (*18*). The enzyme was concentrated to approximately 10 mg/mL in a buffer containing 10 mM sodium cacodylate buffer, pH 6.3, 2 mM DTT, and 3 mM sodium azide. A survey of crystallization conditions was conducted using Crystal Screens I and II from Hampton Research (Laguna Hills, CA). No crystals were obtained in these screens, but a number of test conditions resulted in crystalline-looking precipitate. Analysis of these conditions revealed that acetate, either as the buffer or as an additive, and PEG (of various molecular masses) were common factors. Exploration of these conditions led to the identification of two crystal forms, one grown from 100 mM potassium acetate buffer, pH 4.9−5.4, and 15−18% (w/v) PEG 4000, and a second grown from 100 mM MES buffer, pH 5.7−6.2, 100 mM potassium acetate, and 18−21% PEG 4000.

Crystals of the first form grew as clusters, but it was possible to separate a single crystal from such a cluster and measure diffraction data. The space group is $P1$, with cell dimensions $a = 43.7$ Å, $b = 57.8$ Å, $c = 41.4$ Å, $\alpha = 95.5°$, $\beta = 98.2°$, and $\gamma = 92.7°$, and two molecules per asymmetric unit based on volume considerations (*19*). Data measured from the initial crystal examined had a resolution limit of 2.5 Å. Crystals of the second form were not well shaped, but they were very large. The space group is $P2_1$, with cell dimensions $a = 42.4$ Å, $b = 67.0$ Å, $c = 69.7$ Å, and $\beta = 104.0°$, and two molecules per asymmetric unit. Data measured from the initial crystal examined had a resolution limit of 2.5 Å. Given the higher symmetry of the crystal lattice and the fact that these crystals did not grow in clusters, the monoclinic form was selected for structure determination by heavy-atom isomorphous replacement techniques.

Data Collection and Phasing. All data used in this study were measured from crystals mounted in sealed glass capillaries along with a paper wick wetted with mother liquor. Diffraction data were recorded at room temperature using a Siemens Hi-Star multiwire X-ray area detector mounted on a Supper 3-axis camera at a crystal-to-detector distance of 10 cm. Graphite-monochromated Cu Kα X-radiation was provided by a Rigaku RU-200BH rotating anode generator operated at 50 kV and 180 mA. The data set used in refinement was recorded from a single crystal that measured approximately 2.5 × 0.29 × 0.12 mm. Data were measured as a series of 4-min, 0.25° oscillation frames, with one sweep of 161.5° at $\phi = 0°$ and a second sweep of

[1] Abbreviations: MES, 4-morpholineethanesulfonic acid; PIPES, 1,4-piperazinediethanesulfonic acid; MOPS, 4-morpholinepropanesulfonic acid; MOPSO, β-hydroxy-4-morpholinepropanesulfonic acid; DIPSO, 3-[bis(2-hydroxyethyl)amino]-2-hydroxy-1-propanesulfonic acid; rms, root mean square.

Table 1: Data Collection Statistics

resolution range (Å)	no. of reflections[a]	completeness	mean $Y/\sigma(Y)$[b]	R_{merge}[c]
∞−3.36	5432	0.990	131.6	0.015
3.36−2.67	5308	0.987	49.2	0.028
2.67−2.33	5173	0.962	24.4	0.041
2.33−2.12	4932	0.920	16.6	0.050
2.12−1.97	4713	0.877	11.1	0.060
1.97−1.85	3950	0.739	6.7	0.074
∞−1.85	29508	0.913	42.8	0.032

[a] The number of reflections with $I > \sigma(I)$. [b] Y = average of all observations of a given reflection. [c] $R_{merge} = \sum_{hkl}\sum_i|I(hkl,i) - \langle I(hkl)\rangle|/\sum_{hkl}\sum_i|I(hkl,i)|$.

180° at $\phi = 90°$. The cell constants were $a = 42.27$ Å, $b = 66.96$ Å, $c = 69.48$ Å, and $\beta = 103.77°$, and the data extended to a nominal resolution of 1.85 Å. The statistics for this data set are given in Table 1.

Potential heavy-atom derivatives were prepared by soaking crystals for 1−18 h in solutions that approximated the mother liquor in which the crystals were grown, to which the heavy atom had been added. Six derivatives were identified by examination of difference Patterson or difference Fourier maps. The statistics for the heavy-atom phasing are shown in Table 2.

The electron density map calculated from these phases was of modest quality, even after solvent flattening, and it was hoped that the map could be improved by averaging over the two copies of the protein in the asymmetric unit. A self-rotation function map (*20*), however, did not reveal the orientation of a 2-fold symmetry axis, and attempts to locate such an axis by inspection of the electron density map or by analysis of the positions of the heavy atoms were not successful. Therefore, the backbones of the two molecules in the asymmetric unit were traced, insofar as was possible, in the solvent-flattened MIR map. It was possible to identify many of the structural features of both molecules; the process of tracing was aided by the publication of the structure of the metallo-β-lactamase from *B. cereus* (*4*). Comparison of Figure 3 of Carfi et al. (*4*) with the partial chain tracing for the present structure, combined with analysis of the heavy-atom positions, revealed that the relationship between the two molecules in the asymmetric unit is largely a translational one, with only a 14° rotational component.

Once located, the general operator that relates the two molecules was used to average the electron density map. The quality of the resulting averaged map was higher than that of the unaveraged map, but the tracing of three regions of the polypeptide chain still remained ambiguous. Therefore, three-dimensional α-carbon coordinates were extracted from the stereo diagram in Figure 3 of the structure report of the *B. cereus* enzyme (*4*). The α-carbon tracing of the structure reported here was being adjusted in light of that approximate α-carbon model for the *B. cereus* enzyme when the structure of the unliganded form of this enzyme was reported (*6*). α-Carbon positions were extracted from Figure 1b of Concha et al. (*6*), and the remaining ambiguities in the tracing of this determination of the *B. fragilis* structure were quickly resolved.

Refinement. The early refinement involved numerous cycles of least-squares minimization, manual refitting, and reinterpretation of the chain tracing at 2.5-Å resolution. Once the chain tracing was clarified, the refinement proceeded by alternating cycles of simulated annealing refinement and refitting with reference to $2F_o - F_c$ and simulated annealing omit maps (with 10 residues deleted per map). Only molecule A was refit during the early stages of this process; coordinates for molecule B were generated by rigid-body alignment of the newly rebuilt molecule A to the model of molecule B from the previous refinement cycle. Beyond this implicit imposition of molecular averaging, the two molecules were not constrained to one another during refinement. Higher-angle data were gradually introduced to the refinement, and solvent atoms were added as they were observed in the maps during fitting. During the final two cycles of refitting against simulated annealing omit maps, molecules A and B were fit independently.

Table 2: Multiple Isomorphous Replacement Data Collection and Phasing

derivative	resolution	Data Collection no. of reflections[a]	completeness	mean $Y/\sigma(Y)$[b]	R_{merge}[c]
platinum tetrachloride	2.55	10617	0.837	2.4	0.084
parachloromercuribenzoate	2.25	13730	0.762	5.0	0.042
fluorescein mercuric acetate	2.55	10612	0.849	3.1	0.055
platinum terpyridylchloride	2.55	9960	0.787	2.5	0.057
samarium acetate	3.16	5477	0.836	7.6	0.074
uranium acetate	2.85	8142	0.921	7.0	0.093

derivative	R_{iso}[d]	Phasing mean fom[e]	phasing power[f]	R_{Cullis}[g]	R_{Kraut}[h]
platinum tetrachloride	0.121	0.451	1.82	0.632	0.176
parachloromercuribenzoate	0.082	0.277	1.13	0.706	0.107
fluorescein mercuric acetate	0.094	0.247	1.24	0.718	0.143
platinum terpyridylchloride	0.086	0.172	1.32	0.642	0.132
samarium acetate	0.089	0.266	1.16	0.714	0.131
uranium acetate	0.142	0.301	1.77	0.586	0.209
overall		0.560			
after solvent flattening		0.872			

[a] The number of reflections with $I > \sigma(I)$. [b] Y = average of all observations of a given reflection. [c] $R_{merge} = \sum_{hkl}\sum_i|I(hkl,i) - \langle I(hkl)\rangle|/\sum_{hkl}\sum_i|I(hkl,i)|$. [d] $R_{iso} = \sum|F_{PH} - F_P|/\sum|F_P|$. [e] Mean figure-of-merit. [f] Phasing power $= [\sum|F_{H,calc}|^2/\sum(|F_{PH,obs}| - |F_{PH,calc}|)^2]^{1/2}$. [g] $R_{Cullis} = \sum||F_{PH,obs} \pm F_{P,obs}| - F_{H,calc}|/\sum|F_{PH,obs} \pm F_{P,obs}|$ for centric reflections. [k] $R_{Kraut} = \sum||F_{PH,obs}| - |F_{PH,calc}||/\sum|F_{PH,obs}|$.

As the model improved, it became evident that the active site of the enzyme was not empty; clear density was observed in active sites of both molecules A and B that was interpretable as a molecule of MES, the buffer used in the crystallization mixture. This density was populated with solvent atoms until the X-PLOR phase of the refinement was complete; at that point the resolution was 1.85 Å, the *R*-factor was 0.173 (*R*-free = 0.242), and there were 382 solvent atoms in the model.

The refinement was completed in the program PROLSQ, at which point an atomic model for MES was introduced to each active site. Individual isotropic *B* values were refined for all atoms, and solvent atoms for which *B* refined to 65.0 Å^2 or greater were omitted from the model. The occupancy of all atoms was held fixed at 1.0. The SIGDEL weighting model was used in PROLSQ to set the relative weights applied to structure factor and geometric restraints (SIGDEL $= A + B \sin \theta/\lambda - {}^1/_6$). The values of *A* and *B* were initially set to $A = 22$ and $B = -150$ and were adjusted throughout refinement to maintain the desired quality of geometry; for the final cycle of refinement the values were $A = 19.5$ and $B = -40$.

There was no interpretable density for residues 1−3 at the N-terminus or for residues 231−232 at the C-terminus of either molecule, so coordinates were not fit for those residues. At the beginning of refinement, the amino acid sequence of the metallo-β-lactamase of the TAL3636 strain of *B. fragilis* [CcrA in the nomenclature of Rasmussen and Bush (*3*)] was assumed (Genbank accession code M63556). As refinement proceeded, it became clear that the amino acid sequence of the enzyme studied here, which was cloned from a clinical isolate of *B. fragilis*, differs from that sequence at one position, Thr instead of Ala at residue 171. To confirm this difference, the gene was sequenced, and the amino acid sequence predicted from the nucleic acid sequence does indicate that Thr is present at position 171. A second difference, Asn instead of Asp at position 208, was also predicted from the gene sequence; as these two residues are isosteric, this difference had not been detected during the refinement of the X-ray structure.

In the final model, 352 (90.7%) of the residues are in most favored regions of a Ramachandran plot, 34 (8.8%) are in additionally allowed regions, and no residues are in generously allowed regions. Residue 52 in each molecule (0.5%) is in a disallowed region; a strained main-chain geometry had also been found for this residue in the unliganded structure (*6*) and discussed in terms of the role this residue plays in organizing the active site of the enzyme. One buried solvent atom per molecule refined to a *B*-factor of 2.0 (the lower limit allowed) when treated as an oxygen atom; on the basis of the criteria of bonding distance and coordination outlined by Nayal and Di Cera (*21*), this atom was reassigned as a Na^+ ion. As an example of the quality of the final $2F_o - F_c$ map, the electron density around MES, the two zinc atoms, and the associated solvent atoms is shown in Figure 1 for molecule A. The statistics for the final model are given in Table 3. Coordinates have been deposited with the Brookhaven Protein Data Bank (entry code 1A7T).

Enzyme Assays. Metallo-β-lactamase activity was assessed using the chromogenic substrate nitrocefin (*22*) as has been previously described (*18*); IC_{50} values were determined with nitrocefin at 20 μM, approximately the value of K_m. Stock solutions of MES, 1,4-piperazinediethanesulfonic acid (PIPES), 4-morpholinepropanesulfonic acid (MOPS), and 3-[bis(2-hydroxyethyl)amino]-2-hydroxy-1-propanesulfonic acid (DIPSO) were prepared at 0.40−1.00 M at pH 6.3, 6.9, 7.0, and 7.4, respectively. Enzyme was diluted into 5 mM sodium phosphate buffer, pH 7.3; after the enzyme was incubated at 37 °C for 15 min in the presence of candidate inhibitors, reactions were initiated by addition of nitrocefin. Reported values for K_i were determined using a model for competitive inhibition: $y = v_{max}x_1/(x_1 + K_m(1 + x_2/K_i))$, where y = initial velocity of hydrolysis, x_1 = concentration of nitrocefin, and x_2 = concentration of inhibitor.

RESULTS

Binding of MES to the Active Site. Despite the fact that the two molecules in the asymmetric unit were treated independently in the final cycles of fitting and refinement, they are virtually identical (rms deviation of 0.25 Å for 227 α-carbon pairs). Furthermore, the interactions with MES are so similar that we will limit the discussion here to molecule A. The enzyme consists of two domains of similar topology, with the active site situated at the interface between the domains. MES binds to the active site, in a pocket lined on one side by residues in the active site, and on the other side by residues in the flexible β-strand (flap) of the protein between residues 26 and 36 (Figure 2).

As is illustrated in Figures 1 and 3, coordination of the two zinc atoms remains the same in this inhibited complex as it was in the structure of the unliganded enzyme (*6*); Zn 1 and Zn 2 each have three ligands from the protein, the two zinc atoms share a bridging water (or hydroxyl) molecule (Wat 253), and Zn 2 is coordinated by an additional water molecule (Wat 254) (Figure 3). It is important to note that neither of these water molecules is displaced upon binding of MES. Two of the oxygen atoms of the sulfonic acid group of MES are within hydrogen-bonding distance of Wat 254 (2.3 and 3.4 Å); the third sulfonic acid oxygen forms a hydrogen bond (2.9 Å) with the amide nitrogen of Asn 176. All three sulfonic acid oxygen atoms interact with the terminal nitrogen of the side chain of Lys 167, but the distances (3.7, 3.8, and 3.9 Å) are rather long for hydrogen bonds.

Interactions involving the nitrogen atom of the morpholino group are mediated by a solvent molecule (Wat 647), which coordinates the morpholino nitrogen (3.3 Å), the side-chain nitrogen of Asn 176 (2.8 Å), and Wat 253 (2.7 Å). The morpholino group also forms hydrophobic interactions with the protein, principally with the side chains of residues Ile 29, Trp 32, and Val 35 of the flap. The only interaction with MES that differs between molecules A and B involves the oxygen atom of the morpholino group: in molecule B there is a hydrogen bond between this oxygen and a solvent atom, while in molecule A there is an interaction with the guanadinium group of residue Arg 200 of a symmetry-related molecule B.

Inhibition of the Enzyme by MES. The unanticipated discovery of a molecule of MES bound to the active site led us to test whether MES and other sulfonic acids, illustrated in Figure 4, were in fact inhibitors of the enzyme. MES is

Table 3: Summary of Refined Model

root-mean-square deviation	σ	value in model	no. of restraints total	no. of restraints $>2\sigma$	no. of restraints $>3\sigma$
from ideal bond distances					
bond distances	0.020	0.018	3592	95	8
angle distances	0.030	0.035	4898	352	71
planar 1−4 distances	0.040	0.037	1262	49	5
from ideal planarity (Å)	0.020	0.017	602	7	2
from ideal chirality (Å^3)	0.150	0.166	560	31	6
from permitted contact distances (Å)					
single-torsion contacts	0.500	0.203	1295	2	0
multiple-torsion contacts	0.500	0.201	899	1	0
possible H-bonds	0.500	0.199	273	0	0
from ideal torsion angles (°)					
planar groups (0 or 180)	3.0	2.9	456	16	3
staggered groups (±60 or 180)	5.0	15.5	586	36	6
orthonormal groups (±90)	20.0	22.0	52	2	2

	no. of atoms	mean *B*-factor
protein	3488	14.0
inhibitor	24	27.6
zinc	4	11.1
solvent	337	33.9
sodium	2	36.5
total	3855	15.8

resolution range (Å)	no. of reflections	*R*
10.00−5.46	1084	0.217
5.46−4.19	1526	0.127
4.19−3.52	1896	0.123
3.52−3.10	2190	0.126
3.10−2.80	2412	0.143
2.80−2.57	2630	0.150
2.57−2.39	2765	0.153
2.39−2.25	2921	0.154
2.25−2.12	3019	0.157
2.12−2.02	3096	0.160
2.02−1.93	3006	0.171
1.93−1.85	2722	0.188
10.00−1.85	29267	0.151

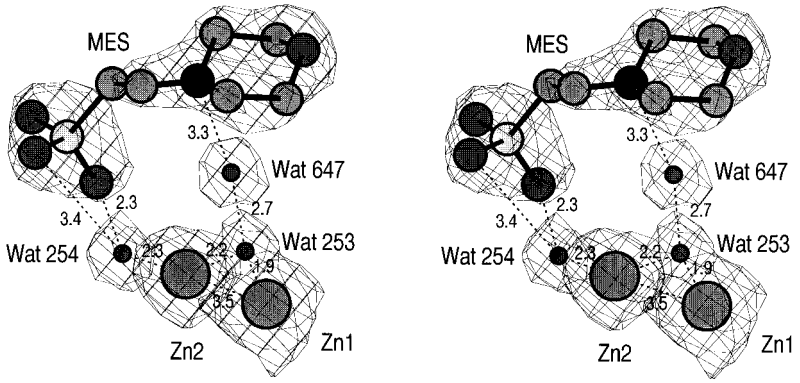

FIGURE 1: Electron density around MES, the two zinc atoms, and associated solvent atoms in molecule A of the complex with the *B. fragilis* metallo-β-lactamase. The $2F_o - F_c$ map, calculated with phases from the final model, has been contoured at 1.0σ. Hydrogen bonds are indicated with dashed lines, and the length of each bond is given.

a competitive inhibitor, with a K_i of 23(± 5) mM. PIPES is also an inhibitor, but it is less potent than MES, with an IC_{50} of 70(±10) mM (the mode of inhibition by PIPES could not be unambiguously determined). PIPES is a larger compound than MES, but graphical fitting of PIPES into the active site of the enzyme indicated that the second ethanesulfonic group of PIPES could easily be accommodated, as it would point away from the pocket in which the single ethanesulfonic acid of MES binds. In this model, the second ethanesulfonic acid group does not make any additional hydrogen bonds, but neither does it form unfavorable steric interactions with the rest of the protein. MOPS and MOPSO both showed weak inhibition, but in each case the IC_{50} was greater than 800 mM, the highest concentration tested; graphical fitting of these compounds into the active site of the enzyme indicates that the bulkier propanesulfonic acid group of MOPS and the 2-hydroxypropanesulfonic acid of MOPSO cannot make the hydrogen bonds available to the ethanesulfonic acid group of MES and PIPES. DIPSO showed no measurable inhibition at 800 mM, the highest

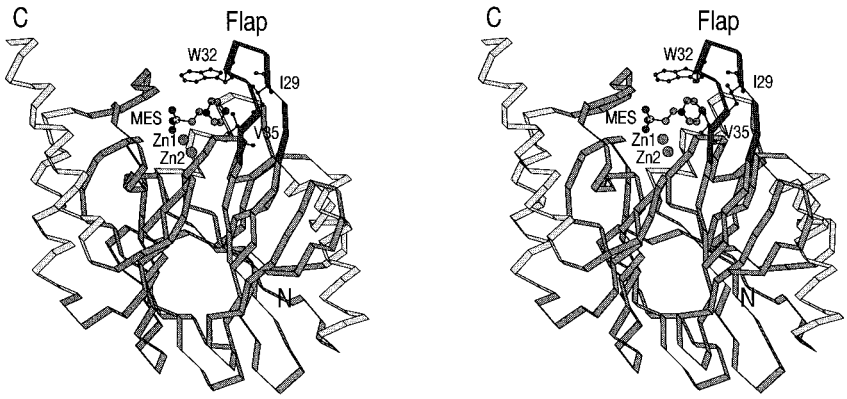

FIGURE 2: The binding of MES to the *B. fragilis* metallo-β-lactamase. The N-terminal domain of the enzyme is to the right in this view, and the C-terminal domain is to the left. The protein is drawn as an α-carbon ribbon, with residues in the flap indicated by dark shading in the ribbon drawing; residues in beta sheets, by medium shading; and residues in helices, by light shading. The zinc atoms are drawn as large spheres, and all atoms are drawn for the molecule of MES and for the three hydrophobic residues in the flap with which it interacts (Ile 29, Trp 32, and Val 35).

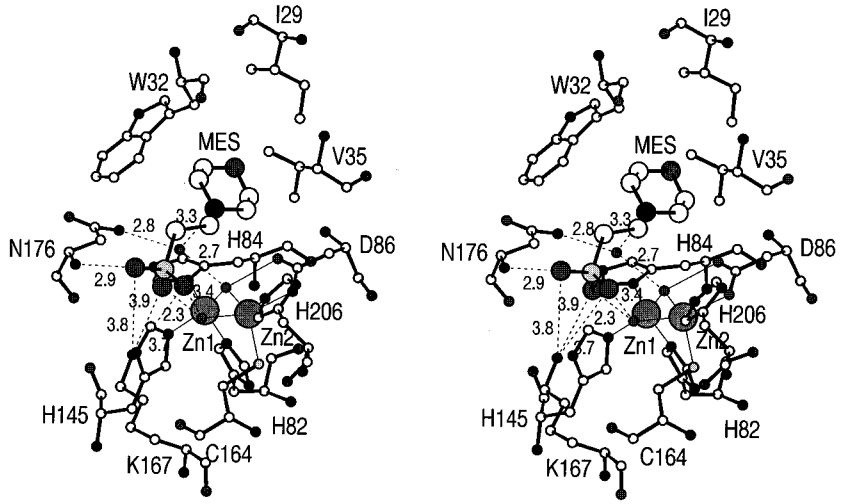

FIGURE 3: Interactions of MES with the *B. fragilis* metallo-β-lactamase. Hydrogen bonds between MES, solvent, and the protein are indicated by dashed lines, with the length of each bond indicated. Bonds between the two zinc atoms (labeled Zn1 and Zn2) and their protein ligands, as well as the two coordinated water atoms, are indicated by solid lines; for clarity, the distances have not been indicated.

concentration tested; this result is not surprising given that this compound also has a 2-hydroxypropanesulfonic acid and that it lacks the morpholino group that mediates hydrogen bonding interactions with the binuclear zinc cluster in the MES complex.

Comparisons between Structures of B. fragilis Metallo-β-lactamases. With three independent structure determinations of the metallo-β-lactamase from *B. fragilis*, each with two molecules per asymmetric unit, we now have six observations of the structure of this protein. We have compared them in a pairwise fashion, using an approach that removes from the rigid-body superposition pairs of α-carbons that differ by more than a user-specified limit, which we have set to 1.0 Å in this study. As shown in Figure 5A and the data in Table 4, the overall agreement of these six structures is very high, with a largest pairwise rms deviation of only 0.55 Å. The deviations that do occur are at the N- and C-termini and in the flaps.

The termini are regions of high thermal factors in all six of the crystallographic observations, to the extent that as many as three residues, depending on the structure, are not sufficiently ordered to be accurately modeled. Most of the termini are involved in crystal packing interactions, so it is not surprising that these are regions where conformational differences are observed. What is a bit surprising is that

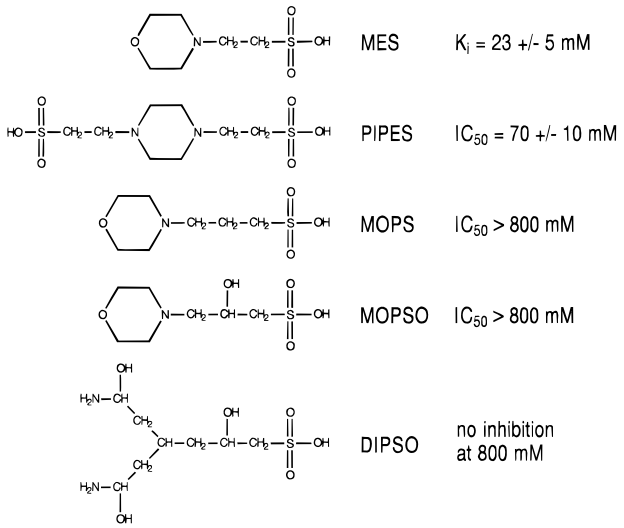

FIGURE 4: The chemical structures of the sulfonic acid buffers studied as potential inhibitors of the *B. fragilis* metallo-β-lactamase. The K_i (or IC_{50}) value for the inhibition of *B. fragilis* metallo-β-lactamase by each of these compounds is indicated.

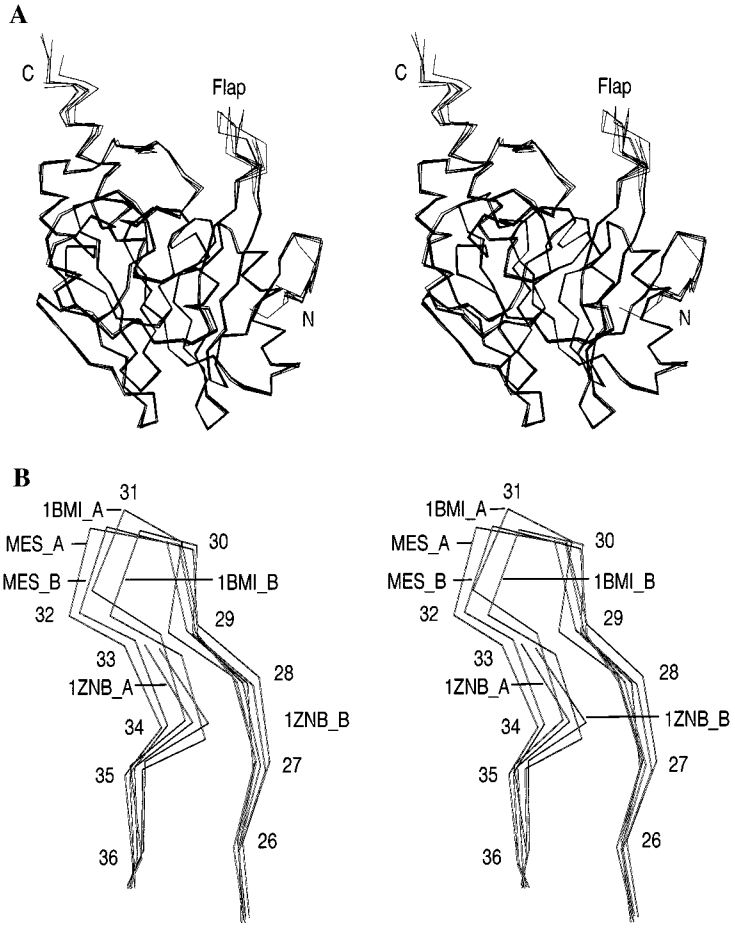

FIGURE 5: The α-carbon backbones of six independent observations of the *B. fragilis* metallo-β-lactamase, two each from three different crystal structure determinations. Molecule A of the MES complex has been taken as the reference, and the other five structures have been aligned with it as described in the text. (A) The complete α-carbon backbones of the six structures; the regions of greatest structural flexibility are at the N- and C-termini and in the flap. (B) A detailed view of the conformation of the flaps in the six molecules. Molecules A and B of the MES complex are labeled MES_A and MES_B; molecules A and B of the tetragonal and orthorhombic forms of the unliganded structures are labeled using their PDB entry codes, which are 1ZNB and 1BMI, respectively.

Table 4: Comparisons between Structures of *B. fragilis* Metallo-β-lactamase

	MES_A		MES_B		1ZNB_A		1ZNB_B		1BMI_A		1BMI_B	
					No. of α-Carbon Pairs Compared and rms Deviation[a]							
MES_A			227	0.25	219	0.31	217	0.37	213	0.33	213	0.31
MES_B	227	0.25			217	0.34	214	0.42	213	0.37	220	0.32
1ZNB_A	225	0.50	225	0.55			223	0.34	216	0.27	219	0.27
1ZNB_B	225	0.45	225	0.50	228	0.52			216	0.38	221	0.40
1BMI_A	227	0.55	227	0.55	226	0.54	226	0.47			214	0.31
1BMI_B	227	0.55	227	0.50	228	0.53	228	0.49	228	0.49		
					α-Carbon Pairs in the Flap That Differ by More Than 1.0 Å and Largest Deviation[b]							
MES_A			none		34	1.3	34	2.0	32	2.0	31	3.4
MES_B	none				30	1.2	34	1.7	32	1.9	31	3.1
1ZNB_A	28, 34		30, 34				30	1.3	30	1.2	33	1.9
1ZNB_B	28, 33−35		28, 30, 33−34		30				30	2.2	33	1.3
1BMI_A	28−34		28−33		29, 30		28−30, 34				31	2.2
1BMI_B	28, 31−34		31−34		30, 33		33		28−34			

[a] The number of α-carbon pairs and the rms value are given for each comparison. Values in the lower left of the table are for all possible α-carbon pairs; values in the upper right represent the results when α-carbon pairs that differ by more than 1.0 Å are removed from the alignment. [b] The values in the lower left of the table are the residue numbers of the α-carbon pairs in the flap that differ by more than 1.0 Å; the values in the upper right are the residue number of the α-carbon pair with the greatest deviation and the magnitude of the deviation, in Å.

the two independent molecules in each of the unliganded structures, which are related by the same 2-fold operator in both cases, differ more from one another than do the two observations in the complex with MES, where the operator that relates the two molecules is a general one. However, when one examines the interactions between monomers in the unliganded dimer (Figure 6), one finds that the dimer interface is formed by β-sheet-type hydrogen bonding between residues 120 and 130, and that the N- and C-termini and the flap of each monomer are all on the exposed outer surface of the dimer and thus subject to distinct crystallographic environments.

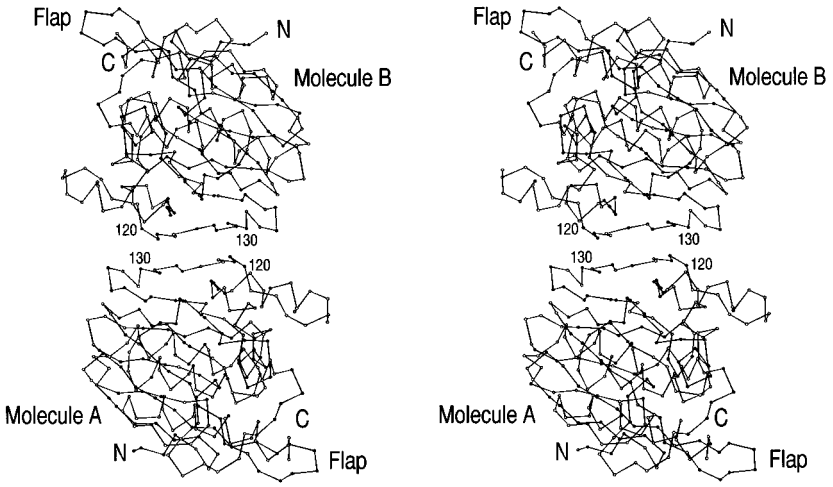

FIGURE 6: The α-carbon backbone of the 2-fold symmetric dimer of *B. fragilis* metallo-β-lactamase observed in both the tetragonal and the orthorhombic structure determination of the unliganded enzyme. The positions of the N- and C-termini and the flap are indicated, and the residues at the beginning and end of the dimer interface (120−130) are labeled.

The most notable structural difference between two independent molecules in the same crystal is found for the first β-turn in the tetragonal form of the unliganded structure, which adopts a completely different conformation in molecules A and B (Figure 5A); the resulting difference in the α-carbon positions of Asp 9 is 4.8 Å. As can be seen in Figure 5A, the conformation of this turn seen in molecule A of the tetragonal unliganded structure is the only observation of this conformation found in the six independent molecules; examination of this region of the structure reveals a favorable interaction of the residues in that turn with equivalent residues in a molecule related by crystallographic 2-fold symmetry.

Of more interest are the conformational differences involving residues in the flap, which are summarized in Table 4 and illustrated in Figure 5B. The two most similar conformations are the two observations of the flap in the MES complex, where the largest α-carbon deviation is 0.7 Å for Glu 30. The two conformations of the flap in the tetragonal form of the unliganded structure are somewhat less closely related (largest deviation = 1.3 Å for Glu 30), but we are limited in our understanding of the conformation of these loops by the disorder at positions 31 and 32. The two conformations of the flap in the orthorhombic unliganded structure are quite different from one another, with the largest deviation being 2.2 Å for Glu 31.

The pair of flaps whose conformations differ the most are in molecule A of the MES complex and molecule B of the orthorhombic form of the unliganded structure. The largest α-carbon deviation for a pair of residues in those flaps is 3.4 Å for Gly 31, and the mean deviation for the nine α-carbon pairs between Ala 27 and Val 35 is 1.6 Å. The pair of flaps with the most similar conformations in two different crystal structures are in molecule B of the MES complex and molecule A of the tetragonal form of the unliganded structure; the largest α-carbon deviation for a pair of residues in those flaps is 1.3 Å for Glu 30, and the mean for the seven residues between Ala 27 and Val 35 is 0.7 Å (only seven α-carbon pairs can be compared because of the disorder at residues 31 and 32 in the tetragonal structure). It should be noted that all four conformations of the flap in the unliganded structures are more distant from the active site than the two conformations observed in the MES complex.

Relationship between the Two Molecules in the Asymmetric Unit. The two molecules in the asymmetric unit of the MES complex are related by a rotation of 14.5° about an axis that is parallel to the crystallographic *b* direction, and a translation of 41.2 Å (Figure 7). Thus the two molecules are nearly parallel, and the interactions that they make with symmetry-related molecules in the crystal are quasi-equivalent; this may in part explain the lack of structural differences induced by crystal lattice effects. The packing of the two molecules is illustrated in Figure 7; the interface involves strand β1 and helix α1 from the N-terminal domain of molecule A and helix α4 from the C-terminal domain of molecule B [using the nomenclature of Carfi et al. (*4*)]. As there is no evidence for a biological role for a dimer of this enzyme, the nonsymmetric dimerization observed here is most likely a crystal-specific interaction, but it is interesting to note that in this inhibited complex the relationship between the two independent molecules is a general one, while in the two different crystallographic observations of the unliganded enzyme the observed dimer is 2-fold symmetric.

DISCUSSION

Flexibility of the Enzyme. Given the different conditions of buffer, pH, and solvent composition under which the crystals of the MES complex and the two unliganded crystal forms of the *B. fragilis* metallo-β-lactamase were grown, the observed structural differences discussed above are remarkably small. The differences at the N- and C-termini are a consequence of different crystallographic environments for those parts of the structure, while the structural differences in the flap reflect crystal packing interactions in the unliganded structures and interactions with an inhibitor in the MES complex. Yet, even given those sources of structural variation, the largest rms difference in α-carbon positions between any pair of molecules compared here is 0.55 Å.

We find in comparing these six observations of the structure in three different crystal forms that there is a significant degree of flexibility in the region of the structure that we refer to as the flap (residues 26−36). There is ample

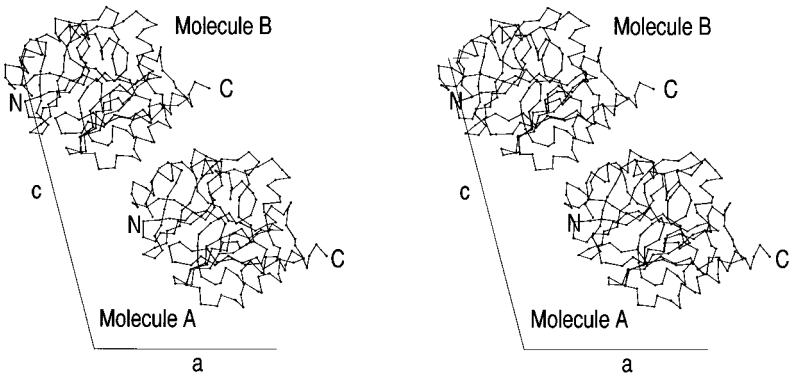

FIGURE 7: The packing of the two molecules in the asymmetric unit of the MES structure. Molecules A and B are labeled, and the positions of the N- and C-termini are indicated. The orientations of the two molecules differ by approximately a 14° rotation about the crystallographic *b* direction, which is perpendicular to the plane of this figure. The orientations of the crystallographic *a* and *c* axes are indicated, and one can see that the 14° difference in orientation of the two molecules corresponds to the difference between the β angle of the crystallographic cell (103.77°) and 90°.

precedent for such mobile regions near the active sites of enzymes, for example, the flap in HIV-1 protease, which adopts a markedly different conformation in complexes with inhibitors than is observed in the unliganded structure (*23*). The conformational changes seen between native and inhibited forms of HIV-1 protease are almost twice as large as the largest deviation in conformation of the flaps that we have seen in this study, but a structural difference of more than 3.0 Å is still a very large one when one is thinking in terms of potential interactions with inhibitors. Furthermore, the conformational differences between unliganded and inhibited forms of the enzyme are of less interest than the possible flexibility available to the flap as it interacts with inhibitors of different structural classes; crystallographic studies with inhibitors of other structural classes are underway, and will be reported elsewhere.

Binding of Sulfonic Acids to Proteins. A review of entries in the Protein Data Bank reveals a small number of structures in which the authors have reported the identification of a molecule of MES or a related sulfonic acid. In some of these cases, the binding site is remote from the active site of the enzyme and is mentioned only in passing in the crystal structure report (*24*, *25*), but in other cases the ethanesulfonic acid acts as a mimic of a substrate or cofactor. In the structure of indole-3-glycerol phosphate synthase from *Solfulobus solfataricus* (*26*), the sulfonic acid moiety of MES binds in a phosphate binding site in the enzyme. In that structure, the ethanesulfonic acid group of MES is well ordered, due to polar interactions with residues that would normally bind phosphate, but the morpholino group is less well ordered. In a second example, MES is found in the active site of dialkyl decarboxylase from *Pseudomonas cepacia* (*27*), adjacent to the position of the bound pyridoxyl-5′-phosphate cofactor. There is a degree of similarity in the observed binding of the sulfonic acid groups in these two structures and the MES−metallo-β-lactamase complex reported here: the pattern of hydrogen bonds involving the oxygen atoms in the sulfonic acid is extensive, and at least one of the oxygen atoms is involved in two different hydrogen bonds. In contrast, the interactions involving the morpholino groups are quite varied. In the active site of dialkyl decarboxylase, the interactions between the morpholino group and the protein are largely hydrophilic, involving packing with the side chains of a tryptophan, a tyrosine, and a leucine residue. In the phosphate binding site of indole-3-glycerol phosphate synthase, the interactions with the morpholino group are predominantly ionic, involving the nitrogen and oxygen atoms of the ring. In neither case is the combination of hydrophobic and polar interactions that we see in the MES−metallo-β-lactamase complex observed, which may explain the greater degree of ordering of the MES molecule in the active site of this enzyme.

Implications for Drug Design. Although we have shown that MES is an inhibitor of the enzyme, it is not in itself a candidate for elaboration into a clinically useful inhibitor, given its observed nonspecific binding to a number of different proteins. However, the determination of the structure in complex with a bound inhibitor has given us an observation of the conformation of the flap in an inhibited complex, and thus a view of the size and shape of the active site in the presence of an inhibitor. This information has been used as a starting point in a series of computational searches for potential inhibitors of the enzyme, the results of which will be reported elsewhere. The flexibility of the flap is an important consideration in designing such searches, as the flap may well adopt other conformations when interacting with inhibitors of different structural classes.

ACKNOWLEDGMENT

We would like to thank our many colleagues for support and encouragement during this work, in particular, Dr. David Pompliano for critical insights into the enzymology aspects of this study, Dr. Barbara Leiting for advice regarding protein expression and purification, Ms. Xiling Yuan for nucleic acid sequencing, and Dr. Joseph Becker for crystallographic advice and thoughtful evaluation of the manuscript.

REFERENCES

1. Buckley, M. M., Brogden, R. N., Barradell, L. B., and Goa, K. L. (1992) *Drugs 44*, 408−444.
2. Turner, P., Edwards, R., Weston, V., Gazis, A., Ispahani, P., and Greenwood, D. (1995) *Lancet 345*, 1275−1277.
3. Rasmussen, B. A., and Bush, K. (1997) *Antimicrob. Agents Chemother. 41*, 223−232.
4. Carfi, A., Pares, S., Duée, E., Galleni, M., Duez, C., Frère, J. M., and Dideberg, O. (1995) *EMBO J. 14*, 4914−4921.

5. Carfi, A., Duée, E., Galleni, M., Frère, J.-M., and Dideberg, O. (1997) Brookhaven Protein Data Bank entry 1BME.
6. Concha, N. O., Rasmussen, B. A., Bush, K., and Herzberg, O. (1996) *Structure 4*, 823−836.
7. Carfi, A., Duée, E., Paul-Soto, R., Galleni, M., Frère, J.-M., and Dideberg, O. (1998*) Acta Crystallogr. D54*, 47−57.
8. Howard, A. J., Gilliland, G. L., Finzel, B. C., Poulos, T. L., Ohlendorf, D. H., and Salemme, F. R. (1987) *J. Appl. Crystallogr. 20*, 383−387.
9. Fitzgerald, P. M. D. (1988) *J. Appl. Crystallogr. 21*, 273−278.
10. Furey, W., and Swaminathan, S. (1997) *Methods Enzymol. 277*, 590−620.
11. Brünger, A. T. (1992) *X-PLOR (Version 3.1): A system for X-ray crystallography and NMR*, Yale University Press, New Haven, CT.
12. Hendrickson, W. A. (1985) *Methods Enzymol. 115*, 252−270.
13. Sack, J. S. (1988) *J. Mol. Graphics 6*, 224−225.
14. Gund, P., Andose, J. D., Rhodes, J. B., and Smith, G. M. (1980) *Science 208*, 1425−1431.
15. Smith, B. M., Hangauer, D. G., Andose, J. D., Bush, B. L., Fluder, E. M., Gund, P., and McIntyre, E. F. (1984) *Drug Inf. J. 18*, 167−178.
16. Pähler, A., and Hendrickson, W. A. (1990) *J. Appl. Crystallogr. 23*, 218−221.
17. Laskowski, R. A., MacArthur, M. W., Moss, D. S., and Thornton, J. M. (1993) *J. Appl. Crystallogr. 26*, 283−291.
18. Toney, J. H., Wu, J. K., Overbye, K. M., Thompson, C. M., and Pompliano, D. L. (1997) *Protein Expression Purif. 9*, 355−362.
19. Matthews, B. W. (1968) *J. Mol. Biol. 33*, 491−497.
20. Crowther, R. A. (1972) in *The Molecular Replacement Method* (Rossmann, M. G., Ed.) pp 173−185, Gordon and Breach, New York.
21. Nayal, M., and Di Cera, E. (1996) *J. Mol. Biol. 256*, 228−234.
22. O'Callaghan, C. H., Morris, A., Kirby, S. M., and Shingler, A. H. (1972) *Antimicrob. Agents Chemother. 1*, 283−288.
23. Fitzgerald, P. M. D., McKeever, B. M., VanMiddlesworth, J. F., Springer, J. P., Heimbach, J. C., Leu, C.-T., Herber, W. K., Dixon, R. A. F., and Darke, P. L. (1990) *J. Biol. Chem 265*, 14209−14219.
24. Eklund, H., Ingelman, M., Söderberg, B.-O., Uhlin, T., Nordlund, P., Nikkola, M., Sonnerstam, U., and Joelson, T. (1992) *J. Mol. Biol. 228*, 596−618.
25. Bujacz, G., Jaskólski, M., Alexandratos, J., Wlodawer, A., Merkel, G., Katz, R. A., and Skalka, A. M. (1995) *J. Mol. Biol. 253*, 333−346.
26. Knöchel, T. R., Hennig, M., Merz, A., Darimont, B., Kirschner, K., and Jansonius, J. N. (1996) *J. Mol. Biol. 262*, 502−515.
27. Toney, M. D., Hohenester, E., Cowan, S. W., and Jansonius, J. N. (1993) *Science 261*, 756−759.

BI9730339